

NiAl formation by annealing of infiltrated aluminium–nickel precursors

D. C. DUNAND

Department of Materials Science and Engineering, Massachusetts Institute of Technology, Cambridge, MA 02139, USA

Samples fabricated by pressure-infiltration of nickel powders with molten aluminium were heat treated at 1200 °C under vacuum or argon isostatic pressure. Reaction and diffusion in the as-infiltrated samples, which contained nickel, aluminium and varying amounts of Ni₂Al₃ and Al₃Ni, resulted in the formation of NiAl as a principal phase with nickel and Ni₃Al as minor phases. All samples exhibited macroporosity due to the formation of an interconnected transient liquid phase during heat treatment. Vacuum-annealed samples also showed extensive Kirkendall porosity in the nickel phase, which was, however, pore-free in hot isostatically pressed samples due to compaction during reaction. Concentration profiles of aluminium in these nickel regions were measured and are in good agreement with predicted values.

1. Introduction

Reactive powder metallurgy – a class of processes whereby a mixture of non-equilibrium powders reacts exothermically to produce a more stable product – has been used to synthesize bulk and reinforced nickel aluminides (NiAl and Ni₃Al) from preforms of elemental nickel and aluminium [1–7]. While reactive powder metallurgy is faster and potentially more economical than the traditional processing routes (casting of molten intermetallic or compaction of aluminide powders), it may yield materials exhibiting residual porosity resulting from (a) adsorbed gases released during rapid heating of the powders, (b) voids in the powder compact and (c) density differences between reactants and products [8]. Further densification during or after reactive powder metallurgy is possible by applying external pressure on the sample [9, 10]. This, however, complicates the process and may also induce breakage of brittle reinforcement used in composites.

In a previous article [11], it was shown that partially reacted, dense aluminium–nickel samples can be produced by pressure-infiltration of coarse nickel powders with molten aluminium. Compared to pressed preforms of mixed metal powders used in the powder-metallurgy processes described above, these dense precursors produced by infiltration offer the advantages of reducing the porosity of the reacted product: degassing of powders is non-existent (solving problem (a) above), and voids in the precursors are eliminated (solving problem (b) above). In this work, we investigated the microstructure resulting from the heat treatment under vacuum or argon isostatic pressure of infiltrated Al–Ni precursors.

2. Experimental procedure

Two infiltrated samples were produced by pressurizing liquid aluminium into preforms of nickel powder

(spherical powders 150–220 µm diameter), as described in detail elsewhere [11]. In short, isothermally-infiltrated sample A resulted from the pressurization (6.9 MPa, argon) of aluminium initially at 685 °C into an evacuated preform containing 60 vol % nickel held at the same initial temperature; sample B resulted from the pressurization (3.6 MPa, argon) of aluminium initially at 765 °C into an evacuated nickel preform containing 51 vol % nickel initially at 285 °C. These cast precursors were cut longitudinally in halves, one of which was examined in the as-cast condition. The other half was further cut longitudinally, resulting in two specimens which were subjected to one of the following heat treatments:

- (i) vacuum annealing at 1200 °C for 40 min;
- (ii) containerless hot isostatic pressing (HIPing) at 1200 °C for 40 min under an argon pressure of 172.5 MPa. Pressurization and heating rates were 2.15 MPa s⁻¹ and 10 °C s⁻¹, respectively.

The as-cast, vacuum-annealed and HIPed samples (designated C, V and H, respectively) were polished and examined by optical microscopy and with an electron microprobe (Jeol Superprobe 733), calibrated with pure nickel and aluminium.

3. Results

Precursor A-C exhibited partially-reacted nickel spheres, representing about 50 vol % of the sample, surrounded with an Ni₂Al₃ reaction zone in a porous Al/Al₃Ni matrix (Fig. 1). After HIPing, these nickel spheres were further consumed to represent in sample A-H about 10 vol % of the initial nickel volume (Fig. 2). A thin layer of about 5 µm of Ni₃Al in contact with nickel-rich NiAl (60 ± 1 at % Ni) surrounds the nickel cores, replacing the Ni₂Al₃ layer found in the as-cast specimen. The space between the original

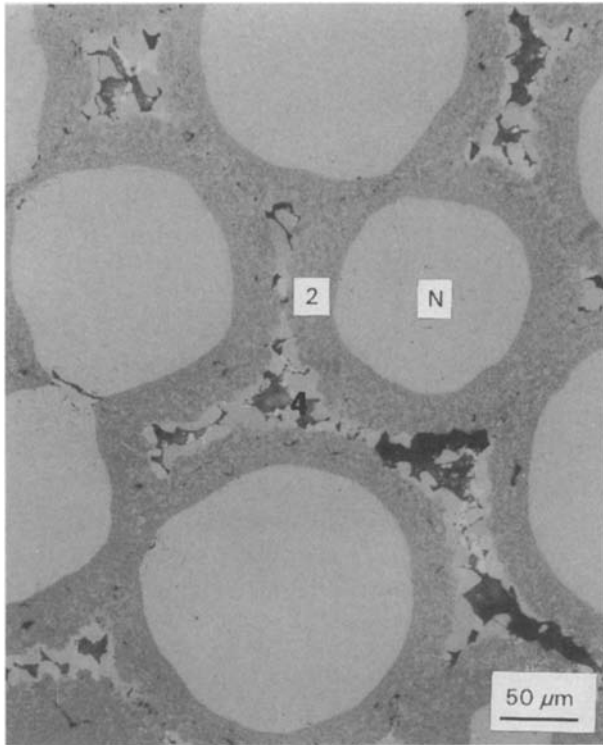


Figure 1 Precursor A-C with nickel spheres (N) surrounded with an Ni_2Al_3 layer (2) in a matrix of Al_3Ni (4) containing some pores.

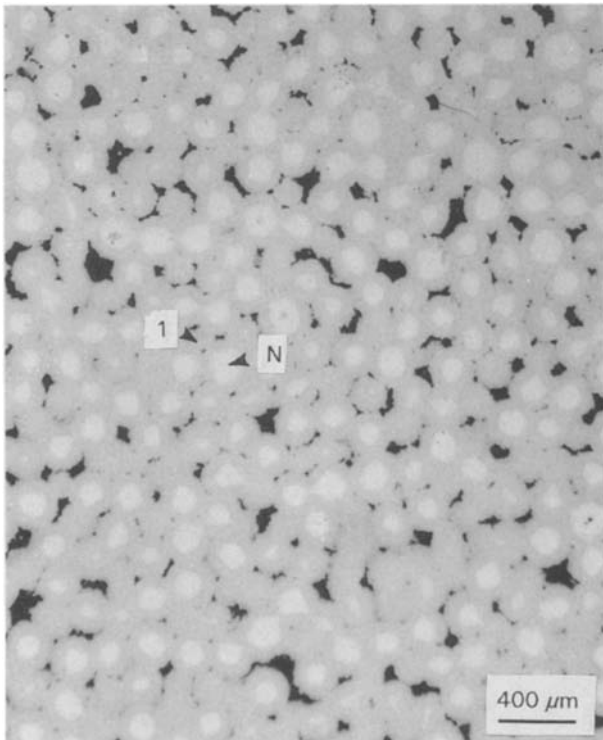


Figure 2 HIPed sample A-H with nickel spheres (N) in an NiAl matrix (1). Pores are visible between the spheres.

nickel spheres, which contained Al_3Ni and aluminium before heat treatment, is composed of pores and nickel-poor NiAl (44 ± 1 at% Ni) far from the Ni_3Al layer. Except for the microporosity described below, the structure of the vacuum-annealed sample A-V is similar to that of the HIPed sample A-H.

The microstructures of the non-isothermally infiltrated precursor B-C consisted of nickel spheres, with two thin reaction layers of Ni_2Al_3 and Al_3Ni (corresponding to about 10 vol% of the initial nickel volume) in a pore-free Al- Al_3Ni eutectic matrix (Fig. 3). After heat treatment, the microstructures of samples B-H and B-V are qualitatively similar to those of samples A-H and A-V, respectively; however, the NiAl matrix of sample B-H tends to be richer in nickel than that of sample A-H (47-64 at%). This is within the single-phase NiAl region at the heat-treatment temperature, but in the two-phase region NiAl/ Ni_3Al at room temperature.

In all heat-treated samples, Ni_3Al was observed decorating NiAl grain boundaries, as the result of precipitation induced upon cooling by a narrowing of the NiAl field. A similar structure was reported by Arkens *et al.* [12] in their HIPed samples of nickel-coated aluminium powders.

4. Discussion

4.1. Intermetallic formation

All samples exhibit a composition closer to equilibrium after heat treatment: the low-melting phases aluminium, Al_3Ni and Ni_2Al_3 were completely absent, the main phase being NiAl, with some remnants of non-equilibrium nickel and Ni_3Al . This structural evolution is qualitatively similar to that observed by Hickl and Heckel [13] who annealed pack-aluminized nickel specimens in argon at 1000 °C: the large Ni_2Al_3 layer which formed initially was consumed by a growing NiAl layer, while the thin layer of Ni_3Al between

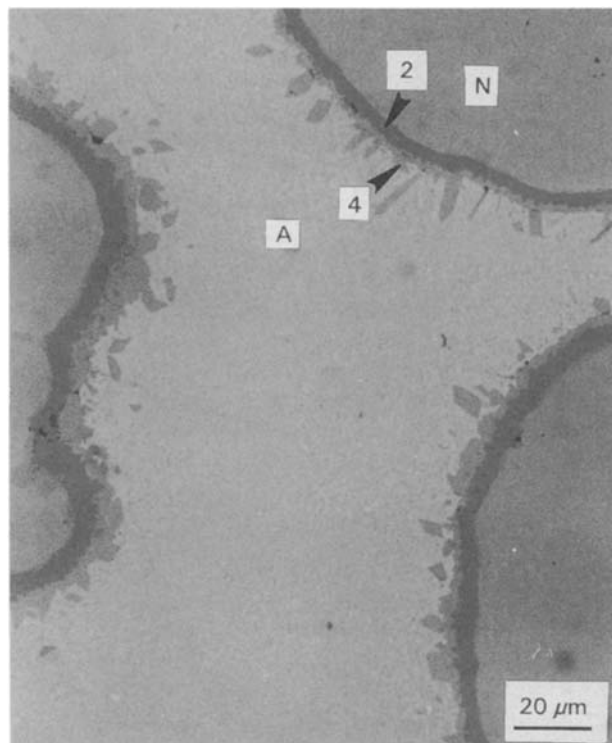


Figure 3 Precursor B-C showing nickel spheres (N) with a thin Ni_2Al_3 layer (2) and primary Al_3Ni (4) in a matrix of Al_3Ni -Al eutectic (A).

the NiAl and the nickel solid solution moved into the nickel without growing appreciably.

The similar extent of reaction after heat treatment between samples A and B, which exhibited different degrees of nickel reaction in the as cast-condition (50 and 10 vol % respectively), is puzzling at first. Extrapolation of data by Hickl and Heckel [13] in the temperature range between 1000 and 1200 °C shows that the kinetics of diffusion are controlled by the flux of atoms through the thickening NiAl layer, rather than the thin Ni₃Al layer. Therefore, as the NiAl phase becomes thicker, the growth kinetics becomes similar, even if the initial Ni₂Al₃ thickness was different. This shows that the extent of reaction of the as-cast precursors has a minor effect on the time needed to fully convert the samples to NiAl for the experimental conditions used in this study.

4.2. Aluminium diffusion

The partially reacted nickel spheres in the heat-treated samples A and B exhibit a concentration gradient of aluminium between their surface and their centre, where no aluminium could be detected. Fig. 4 shows, for sample B-H, the composition profiles for two different nickel spheres of large apparent radii ($R = 105$ and $125 \mu\text{m}$), which were intersected by the plane of polish near an equatorial plane.

The chemical interdiffusion coefficient, \tilde{D} , at 1200 °C for aluminium concentrations between $c = 0.01$ and 0.17 was measured by Yamamoto *et al.* [14] and can be represented by

$$\tilde{D} = \tilde{D}_0 \exp(8.27c) \quad (1)$$

where $\tilde{D}_0 = 5.6 \times 10^{-14} \text{ m}^2 \text{ s}^{-1}$ is the chemical interdiffusion coefficient extrapolated for $c = 0$. This value compares well to a value of $6.1 \times 10^{-14} \text{ m}^2 \text{ s}^{-1}$ at 1200 °C reported in [15] for aluminium concentrations between 0 and 0.007 and a value of 5.7

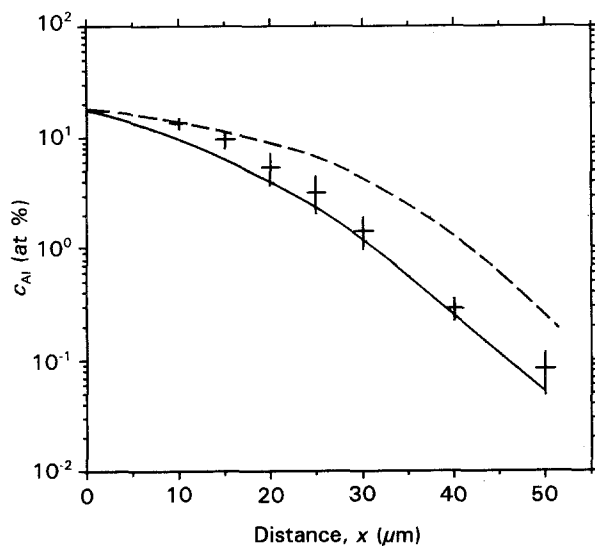


Figure 4 Average aluminium concentration as a function of the distance from the Ni–Ni₃Al interface measured by microprobes at two different locations of two nickel spheres in sample B-H (error bars correspond to one standard deviation). Curves are calculated from Equations 2 (continuous) and 3 (dashed).

$\times 10^{-14} \text{ m}^2 \text{ s}^{-1}$, extrapolated from data measured by Hickl and Heckel [13] with Ni/Ni₃Al diffusion couples between 870 and 1000 °C.

The present problem of spherical diffusion with a moving interface and a concentration-dependent interdiffusion coefficient can be simplified by assuming a stationary planar interface, because $\tilde{D}t/R^2$ is small for the experimental diffusion time, t , of 2400 s and the above values of sphere radius, R , and interdiffusion coefficient. Fig. 4 shows the solution for diffusion in a semi-infinite medium with a concentration-independent diffusion coefficient taken as $\tilde{D} = \tilde{D}_0 = 5.6 \times 10^{-14} \text{ m}^2 \text{ s}^{-1}$

$$c = c_{\max} \left\{ 1 - \operatorname{erf} \left[\frac{x}{2(\tilde{D}t)^{1/2}} \right] \right\} \quad (2)$$

where x is the distance from the interface and $c_{\max} = 0.175$ is the aluminium surface concentration, taken as the solid solubility of aluminium in nickel at 1200 °C [16]. This value is corroborated by STEM profile measurements of NiAl–Ni diffusion couples annealed at 1100 °C for 15 min for which an Ni₃Al layer was formed: at the nickel side of the Ni₃Al–Ni interface, the solid solubility limit was indeed reached [17]. Fig. 4 shows that experimental data at low aluminium concentration is in good agreement with Equation 2.

Equation 2 with $\tilde{D} = \tilde{D}_0$ underestimates the aluminium concentration for small diffusion distances and high aluminium concentrations, because the chemical interdiffusion coefficient given by Equation 1 increases with aluminium concentration. A better estimate of the concentration profile at high aluminium concentrations is given by the general diffusion equation in a semi-infinite medium

$$\frac{\partial c}{\partial t} = \tilde{D} \left(\frac{\partial^2 c}{\partial x^2} \right) + \frac{\partial \tilde{D}}{\partial c} \left(\frac{\partial c}{\partial x} \right)^2 \quad (3)$$

where the chemical interdiffusion coefficient is given by Equation 1. Using the numerical scheme given by Crank [18], we plot in Fig. 4 the solution of Equation 3 for a stationary interface with concentration equal to $c_{\max} = 0.175$. Good agreement is found between Equation 3 and measurements at high aluminium concentration.

The above diffusion solutions overestimate the actual concentration profile, because the moving interface is not taken into account. As the interface with concentration c_{\max} moves towards the centre of the nickel sphere which is aluminium free, the actual composition can be expected to drop faster as a function of the distance than calculated for the case of a stationary interface. Other causes for error originate from experimental conditions (temperature variations, diffusion during heating and cooling, precision of microprobe measurement) and physical data (uncertainties in the measurement of \tilde{D} and its pressure-dependence, assumed to be zero).

4.3. Porosity

The composition of the vacuum-annealed samples shows no major difference with that of their HIPed

counterpart. However, samples A-V and B-V exhibit extensive microporosity at the nickel interface after vacuum heat-treatment (Fig. 5), unlike the HIPed samples. In many cases, the pores coalesced into large gaps, effectively separating the nickel spheres from the rest of the matrix (Fig. 6). This porosity can be explained based on the result of a study by Janssen and Rieck [19] who examined planar diffusion couples in the nickel–aluminium system. They reported that in Al–Ni couples, aluminium atoms diffused rapidly to form a thin layer of Al_3Ni and a thick layer of Ni_2Al_3 , leaving pores in the aluminium. In Ni_2Al_3 –Ni couples, however, the nickel atoms were the mobile species: they diffused from the nickel phase to the Ni_2Al_3 layer where new nickel-rich intermetallic phases were created, while Kirkendall pores were formed in the nickel phase. In both as-cast precursors A and B, each nickel sphere is surrounded by a layer of Ni_2Al_3 itself surrounded by an interconnected aluminium-rich phase (Al_3Ni or Al– Al_3Ni eutectic). Each nickel sphere thus forms a diffusion couple with the matrix. Upon heat treatment, aluminium from the aluminium-rich phase first diffused to form a thick Ni_2Al_3 layer. After elimination of the aluminium-rich phase (resulting in large gaps between the nickel spheres), the system can be considered as a Ni_2Al_3 –Ni couple. Nickel atoms from the nickel spheres then diffused radially outwards into the Ni_2Al_3 layer, forming NiAl and leaving Kirkendall pores in the nickel sphere (Fig. 7a). As the Ni– Ni_3Al interface moved radially towards the centre of the nickel sphere, these Kirkendall pores became part of the intermetallic layer (Fig. 7b). When the voids formed a continuous gap (Fig. 7c), the nickel diffusion flow was locally interrupted. As a result, the Ni_3Al

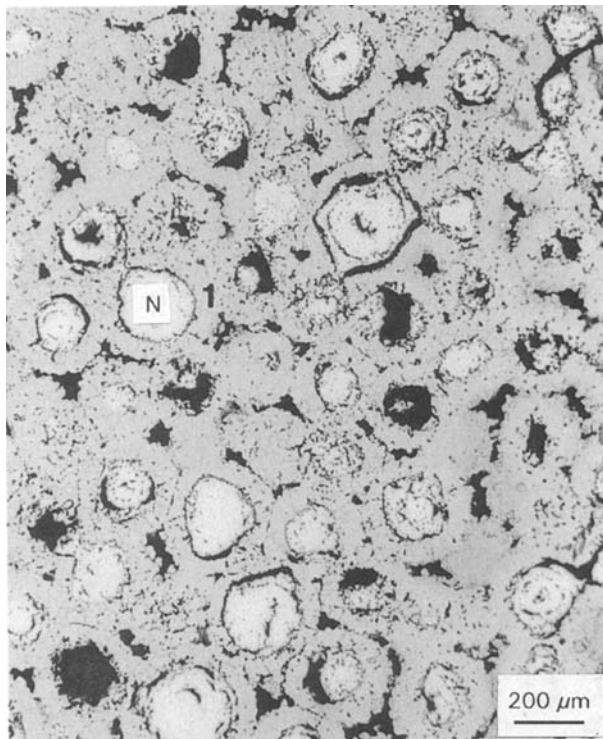


Figure 5 Vacuum-annealed sample A-V showing extensive Kirkendall porosity in the nickel (N) phase. Pores are also visible within the NiAl (1) matrix. Some of the nickel spheres were lost during metallographic preparation.

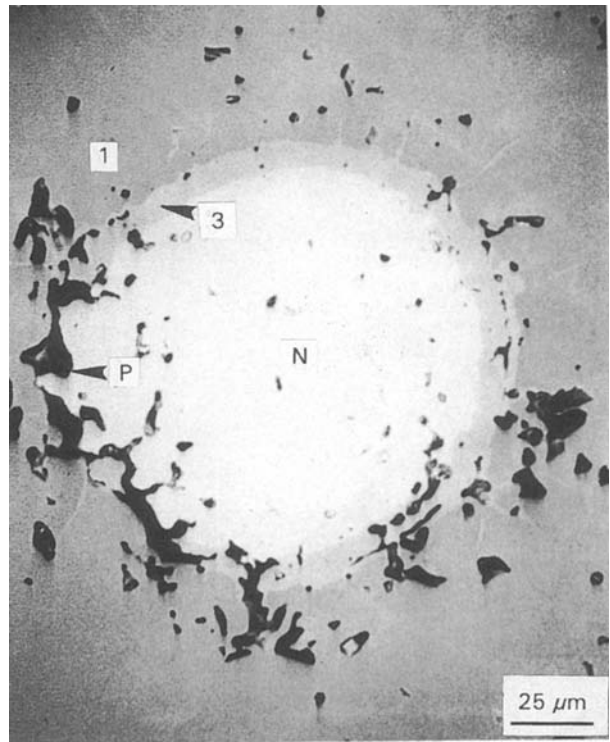


Figure 6 Microprobe picture of the vacuum-annealed sample A-V showing a nickel sphere (N) in the NiAl matrix (1). The thin Ni_3Al layer (3) is absent where pores (P) form an uninterrupted gap between the nickel phase and the matrix.

layer, which was dissolving at the NiAl interface and forming at the nickel interface, disappeared by reaction with the NiAl phase. Fig. 6 illustrates this phenomenon: one side of the nickel sphere is separated from the matrix by coalesced pores and no Ni_3Al layer is visible; the other side is still in contact with the matrix and exhibits an Ni_3Al layer separating the nickel sphere from the NiAl matrix.

A further cause for the microporosity at the Ni/ Ni_3Al interface is the change of volume associated with the formation of the intermetallic phases, which are denser than the volume average of the parent metals. The initial intermetallic layer around the spheres forms a continuous three-dimensional skeleton in the sample. Owing to its rigidity, it is incapable of shrinking to stay in contact with the nickel spheres as the reaction proceeds and as the resulting volume difference increases.

While Kirkendall pores within the nickel spheres are absent in the HIPed samples, the interconnected porosity between the initial nickel spheres is not eliminated by HIPing (Figs 2 and 5). This can be explained in the following manner: as the temperature increased during HIPing, the low-melting, aluminium-rich phase formed an interconnected liquid phase permeating a rigid skeleton of partially reacted nickel spheres. The argon hydrostatic pressure was therefore transmitted to the liquid with no macroscopic compaction of the sample. However, both the liquid, and later the argon replacing the liquid due to depletion by reaction with the solid intermetallic skeleton, were capable of compacting each individual sphere, because the Kirkendall pores they contained were not connected to their surfaces. Because the lack of overall

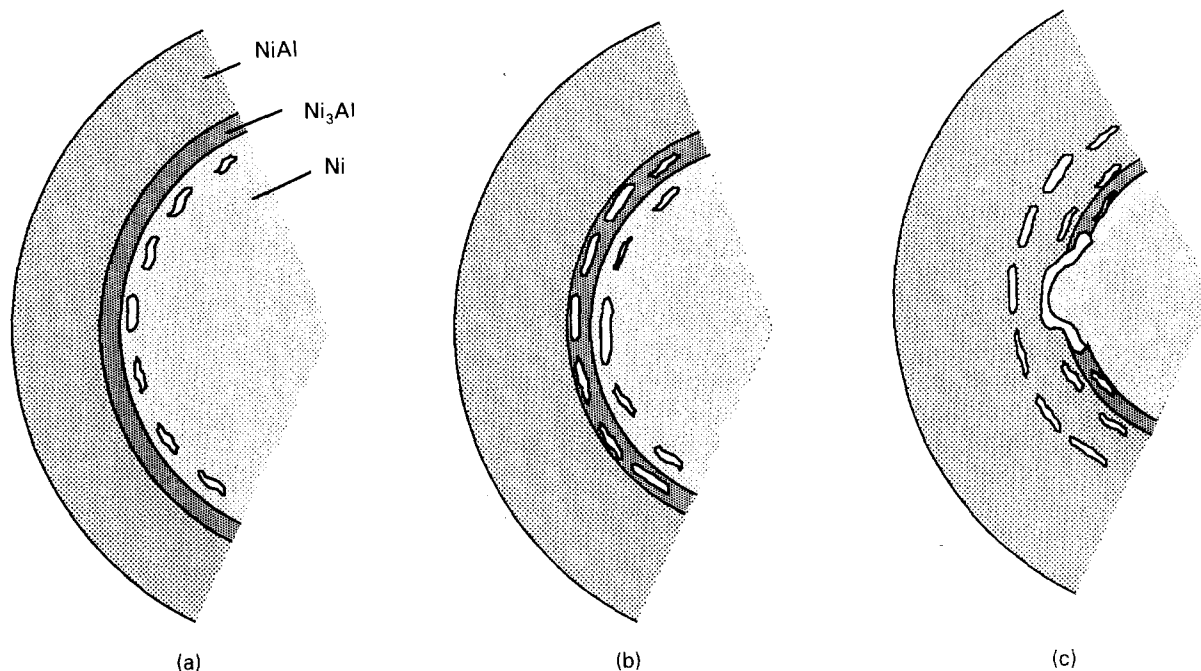


Figure 7 Schematic illustration of Kirkendall pore formation. (a) Pores are formed in the nickel as a result of nickel atoms diffusing radially towards the NiAl layer; (b) as the interface progresses towards the centre of the sphere, the original pores are engulfed in the aluminide layers. New pores form continuously in the nickel phase; (c) upon pore coalescence, the flux of nickel atoms is interrupted. The Ni₃Al dissolves at this location. This illustrates the situation shown in Fig. 6.

compaction seems to be due to the formation of an interconnected liquid phase in contact with the hydrostatic gas, encapsulation of these precursors would probably result in pore-free samples.

5. Conclusions

Aluminium-infiltrated nickel powder samples were heat treated at 1200 °C in vacuum or under an argon hydrostatic pressure of 172.5 MPa, resulting in the formation of the equilibrium phase NiAl together with minor amounts of nickel and Ni₃Al.

The aluminium concentration in the remaining nickel phase was measured as a function of distance from the nickel–nickel aluminide interface. The measured diffusion profile is well described by diffusion solutions assuming a constant interdiffusion coefficient at low aluminium concentrations and large distances and a concentration-dependent coefficient at high aluminium concentration and short distances.

Pores in the vacuum-annealed samples were formed at two locations: (i) between the nickel regions, as a result, of the disappearance by diffusion and reaction of an aluminium-rich liquid phase, and (ii) within the nickel phase, due to the Kirkendall effect. Containerless hot isostatic pressing prevented the latter type of pores, but not the former.

Acknowledgements

The author thanks the Swiss National Science Foundation for a fellowship and Professor A. Mortensen, MIT, for numerous helpful discussions. Partial support from the National Science Foundation (grant MSS-9201843) is also acknowledged.

References

1. D. C. DUNAND, *Mater. Manuf. Proc.*, in print.

2. D. M. SIMS, A. BOSE and R. M. GERMAN, *Prog. Powder Metall.* **43** (1987) 575.
3. Z. A. MUNIR, *Ceram. Bull.* **67** (1988) 342.
4. A. BOSE, B. H. RABIN and R. M. GERMAN, *Powder Metall. Int.* **20** (1988) 25.
5. D. L. ANTON, in "High Temperature/High Performance Composites", edited by F. D. Lemkey, S. G. Fishman, A. G. Evans and J. R. Strife (MRS, Pittsburgh, PA 1988) pp. 57–64.
6. N. S. STOLOFF and D. E. ALMAN, *MRS Bull.* **15** (1990) 47.
7. R. M. GERMAN, in "1990 Advances in Powder Metallurgy", edited by E. R. Andreotti and P. J. McGeehan (American Powder Metallurgy Institute, Princeton, NJ, 1990) pp. 115–32.
8. S. D. DUNMEAD, Z. A. MUNIR, J. B. HOLT and D. D. KINGMAN, *J. Mater. Sci.* **26** (1991) 2410.
9. D. E. ALMAN and N. S. STOLOFF, *Int. J. Powder Metall.* **27** (1991) 29.
10. C. NISHIMURA and C. T. LIU, *Scripta Metall. Mater.* **26** (1992) 381.
11. D. C. DUNAND, J. L. SOMMER and A. MORTENSEN, *Metall. Trans.* **24A** (1993) 2161–70.
12. O. ARKENS, L. DELAHEY, J. D. TAVERNIER, B. HUYBRECHTS, L. BUEKENHOUT and J. C. LIBOUTON, in "High-Temperature Ordered Intermetallic Alloys III", edited by C. T. Liu, A. I. Taub, N. S. Stoloff and C. C. Koch (MRS, Pittsburgh, PA, 1989) pp. 493–8.
13. A. J. HICKL and R. W. HECKEL, *Metall. Trans.* **6A** (1975) 431.
14. T. YAMAMOTO, T. TAKASHIMA and K. NISHIDA, *J. Jpn Inst. Metals* **44** (1980) 294.
15. E. A. BRANDES (Ed.) "Smithells Metal Reference Handbook" (Butterworth, London, UK, 1983).
16. M. HANSEN and K. ANDERKO, in "Constitution of Binary Alloys" (McGraw-Hill, New York, NY, 1958) pp. 118–21.
17. J. I. GOLDSTEIN, M. R. NOTIS and A. D. ROMIG, in "ASM Handbook Vol.10, Materials Characterization", edited by W. E. Whan (ASM, Metals Park, OH, 1986) pp. 476–8.
18. J. CRANK, in "The Mathematics of Diffusion", 2nd Edn (Oxford Science, Oxford, UK, 1975) pp. 116–17.
19. M. M. P. JANSSEN and G. D. RIECK, *Trans. AIME* **239** (1967) 1372.

Received 1 December 1992
and accepted 29 March 1993